

LETTER TO THE EDITOR

Reading diffraction images in strong field ionization of diatomic molecules

To cite this article: Michael Spanner *et al* 2004 *J. Phys. B: At. Mol. Opt. Phys.* **37** L243

View the [article online](#) for updates and enhancements.

You may also like

- [Super-resolution X-ray imaging with hybrid pixel detectors using electromagnetic source stepping](#)
T. Dreier, U. Lundström and M. Bech
- [A spatial-temporal-spectral blending model using satellite images](#)
L Zhang, D Fu, X Sun et al.
- [Analysis of angular resolution and range resolution on multibeam echosounder R2 Sonic 2020 in Port of Tanjung Perak \(Surabaya\)](#)
R N A Oktavia, D G Pratomo and Khomsin



Easy-to-use and Helium-3 free
cryogenics solutions



LEARN MORE

LETTER TO THE EDITOR

Reading diffraction images in strong field ionization of diatomic molecules

Michael Spanner^{1,3}, Olga Smirnova², Paul B Corkum³
and Misha Yu Ivanov³

¹ Department of Physics, University of Waterloo, Ontario N2L 3G1, Canada

² Photonics Institute, Vienna University of Technology Gusshausstrasse 27/387, A-1040 Vienna, Austria

³ National Research Council of Canada, 100 Sussex Drive, Ottawa, Ontario K1A 0R6, Canada

E-mail: mspanner@sciborg.uwaterloo.ca, olga.smirnova@tuwien.ac.at, paul.corkum@nrc.ca
and misha.ivanov@nrc.ca

Received 15 April 2004

Published 27 May 2004

Online at stacks.iop.org/JPhysB/37/L243

DOI: 10.1088/0953-4075/37/12/L02

Abstract

We present a theoretical analysis of how intense, few-cycle infrared laser pulses can be used to image the structure of small molecules with nearly 1 fs temporal and sub-Å spatial resolution. We identify and analyse several physical mechanisms responsible for the distortions of the diffraction image and describe a recipe for recovering an un-distorted image from angle and energy-resolved electron spectra. We also identify holographic patterns in the photoelectron spectra and discuss the requirements to enhancing the hologram resolution for imaging the scattering potential.

(Some figures in this article are in colour only in the electronic version)

Intense laser pulses can generate a diffraction image of a molecule using the molecule's own electrons [1–3], with sub-Å spatial and nearly 1 fs temporal resolution. After strong-field ionization, the electron wave packet is first pulled away from the ion by the electric field of the laser. Within the same laser cycle, the electric field reverses its direction and the electron can be driven back to recollide with the parent ion. Elastic scattering takes the diffraction image of the parent molecule (figure 1) [2].

From the ion's perspective, during the recollision the electron current density exceeds 10^{10} A cm⁻² and is concentrated within a small fraction of the laser cycle (<1 fs) [3], exceeding these characteristics in conventional approaches to ultrafast electron diffraction (see, e.g., [4]) by many orders of magnitude. Energy W of the returning electron reaches $3.17U_p$ [5], where $U_p = E^2/4\omega^2$ is the average electron oscillation energy and E , ω are the field amplitude and

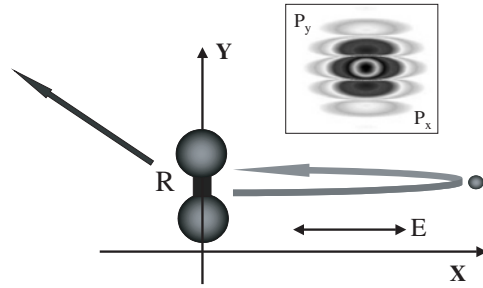


Figure 1. Diffraction during strong-field ionization. The inset sketches ground state in the velocity space, with shades of grey coding the probability.

frequency, respectively (atomic units are used everywhere). For the Ti:sapphire laser $W \approx 133$ eV at the intensity $I \approx 7 \times 10^{14}$ W cm $^{-2}$ and increases proportional to λ^2 with increasing the wavelength λ , yielding sub-Å spatial resolution. A laser pulse can also be used to align [6] molecules, emphasizing the diffraction pattern.

These advantages do not come for free: the nature of the electron pulse and the presence of the strong laser field lead to several complexities. We identify and analyse them numerically and analytically and describe the procedures for recovering the undistorted diffraction image. The main ingredients in our recipe are (i) tunnel ionization regime, (ii) special cuts in the photo-electron spectra and (iii) the use of nearly single-cycle pulses $E(t) \cos(\omega t + \varphi)$ with stabilized carrier-envelope phase φ . Yurchenko *et al* [7] describes three-dimensional *ab initio* numerical simulations which demonstrate how the internuclear distance for diatomics can be identified in the multiphoton regime. Our paper suggests a general recipe for obtaining the overall diffraction image.

We use an example of a diatomic molecule aligned perpendicular to the field $E \cos \omega t$ polarized along the x axis, see figure 1. Numerically, we use the same H_2^+ -like 2D model as in [2] with the soft-Coulomb electronic potential ($a = 0.5$ au)

$$V_M(x, y|R) = V_A(x, y - R/2) + V_A(x, y + R/2) \\ = -\frac{1}{\sqrt{x^2 + (y - \frac{R}{2})^2 + a^2}} - \frac{1}{\sqrt{x^2 + (y + \frac{R}{2})^2 + a^2}}. \quad (1)$$

The internuclear distance is frozen at $R = 4$ au ($I_p = 0.96$ au). Reading the recollision induced diffraction image forces one to deal with several unavoidable complexities outlined below.

- (1) *Imprint of the initial state during tunnelling.* Consider the limit of tunnel ionization $\gamma^2 = I_p/2U_p \ll 1$, where I_p is the ionization potential. For each moment of ionization t_0 , the newly created electronic wave packet in the continuum $\Delta\Psi(\mathbf{v}_\perp, t_0)$ depends on the transverse velocity \mathbf{v}_\perp as (see, e.g., [8]):

$$\Delta\Psi(\mathbf{v}_\perp, t_0) \propto \langle \mathbf{v}_\perp | \Psi_i \rangle \exp\left(-\frac{v^2}{2} \tau_T(t_0)\right) \quad (2)$$

Here $\tau_T(t_0)$ is the tunnelling time, $\omega\tau_T(t_0) \cos \omega t_0 = \gamma$. The Gaussian shape due to tunnelling filters the Fourier-transform $\langle \mathbf{v}_\perp | \Psi_i \rangle$ of the initial orbital Ψ_i which already carries imprint of the orbital's structure (figure 1, inset). This distorts the shape of the ionizing wave packet. We choose laser parameters to minimize such distortions.

- (2) *Holographic-type structures.* The nonzero width of the Gaussian velocity distribution $\Delta v \sim 1/\sqrt{\tau_T}$ equation (2) gives rise to a holographic-type interference in the final electron spectrum. For example, the deflection of the electron recolliding with the velocity $\mathbf{v} \parallel \mathbf{x}$ creates transverse component v_\perp after the scattering. If v_\perp is within Δv , the scattered wave will interfere with the reference wave that has started with nonzero v_\perp and has missed the ion. Similar interference occurs for an atom.
- (3) *Large scattering angles.* For typical recollision energies ~ 100 eV, deflection with relevant transverse velocities $v_\perp \sim \pi/R$ corresponds to large scattering angles θ . Quickly decreasing cross sections $d\sigma(\theta)$ distort the diffraction image.
- (4) *Distortions induced by the laser field.* After the scattering, the electron's longitudinal velocity is changed by the laser field while the transverse velocity remains unaffected. Therefore, for a given recollision energy, the electron's final energy after the 'elastic' scattering depends on the deflection angle. An angle-resolved spectrum for a fixed final energy *does not* correspond to the diffraction pattern for a given recollision energy.
- (5) *Interference between diffraction images taken at different energies.* The recollision energy ranges from 0 to $\sim 3.2U_p$ [5]. In the absence of the laser field, energy-resolved spectra would discriminate between the diffraction images taken at different energies. However, in the presence of a laser field, electrons recolliding with different energies at different times t may end up with the same final velocity vector \mathbf{v} . The resulting interference is caused exclusively by the laser field.

The first step in recovering the diffraction pattern is to account for the laser-induced change in the electron energy after the scattering. In the strong low-frequency field, a large electron oscillation amplitude $\alpha = E/\omega^2$ ($\alpha \approx 40$ au at $I \approx 7 \times 10^{14}$ W cm $^{-2}$ and $\lambda = 800$ nm) separates the recollision into three stages: (i) electron approach with the velocity v , (ii) fast recollision during an interval $\Delta t \sim R/v$ much shorter than the laser cycle (in a quarter-cycle the electron covers the distance $\alpha \gg R$) and (iii) free oscillation in the laser field after the recollision. Since $\omega\Delta t \ll 1$, scattering occurs at a well-defined phase $\phi = \omega t$ and velocity $v(t)$. Without the laser field, the elastic scattering means $v_x^2 + v_y^2 = v^2$, where v is the incoming velocity and v_x, v_y are the parallel and perpendicular velocities after the scattering. The laser-induced oscillation changes this to

$$(v_x - v_0 \sin \omega t)^2 + v_y^2 = v^2(t), \quad v_0 = E/\omega \quad (3)$$

where v_x, v_y are the *final* velocities at the detector and $v(t)$ is the incoming velocity (along the x -axis). Equation (3) assumes fast collision and means that the diffraction image taken at a given energy $v(t)^2/2$ lies on the circular cut through the electron spectrum with the radius $v(t)$ and the origin shifted by $v_0 \sin \omega t$. Each time period of the recollision defines its own circle (both the radius and the shift); the overall spectrum is their superposition.

The simple recollision model [5] assumes that after tunnelling at t_0 the trajectory starts near the origin with negligible velocity. In this model $v(t) = v_0(\sin \omega t_0 - \sin \omega t)$ and the time of ionization t_0 corresponding to t is given by

$$\omega(t - t_0) \sin \omega t_0 + (\cos \omega t - \cos \omega t_0) = 0. \quad (4)$$

Equation (4) means that at t the electron returns to its initial position at t_0 . However, after tunnelling the electron appears at some distance $x(t_0)$ from the origin. For a given recollision moment t , this changes the recollision energy. In the tunnelling limit the correction is [9] $v^2(t)/2 \Rightarrow v^2(t)/2 - I_p dt_0/dt$, where $t_0(t)$ is still defined by equation (4). The cut in the electron spectrum for a given recollision energy from equation (3) becomes

$$(v_x - v_0 \sin \omega t)^2 + v_y^2 = v_0^2(\sin \omega t_0 - \sin \omega t)^2 - 2I_p \frac{dt_0}{dt} \quad (5)$$

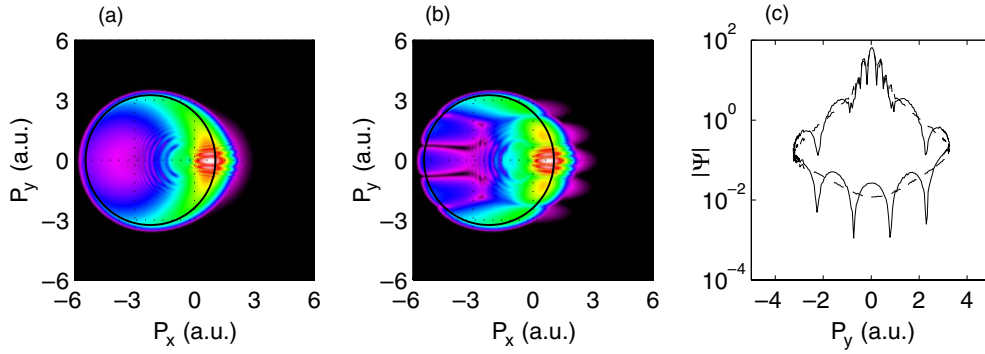


Figure 2. Recollision-induced diffraction for a single phase of birth. (a) Reference signal $|\Psi(v_x, v_y)|$ for a model atom, each new colour corresponds to the next order of magnitude; (b) $|\Psi(v_x, v_y)|$ for a model diatomic molecule; (c) circular cuts for the atom (dashed) and the molecule (solid).

or, introducing dimensionless velocity $\mathbf{u} \equiv \mathbf{v}/v_0$,

$$(u_x - \sin \omega t)^2 + u_y^2 = (\sin \omega t_0 - \sin \omega t)^2 - \gamma^2 \frac{dt_0}{dt}. \quad (6)$$

For the most energetic ($\simeq 3.17U_p$) trajectories $dt_0/dt \simeq -0.32$: the correction is small in the tunnelling regime.

To check this simple recipe for removing the effect of the laser field, we simulate rescattering for a single phase of birth $\omega t_0 = 17^\circ$, which corresponds to the maximum return energy. First, we propagate a classical trajectory starting at the ‘exit’ of the tunnelling barrier $x_0 \approx I_p/E \cos \omega t_0$ from $\omega t_0 = 17^\circ$ to the zero of the laser field $\omega t^* = \pi/2$. The position and velocity of the trajectory at $\omega t^* = \pi/2$ is used to initialize a Gaussian wave packet which is then propagated by solving the time-dependent Schrödinger equation in 2D for the model molecule equation (1), starting at $\omega t^* = \pi/2$. The wave packet width is set equal to that found by solving the Schrödinger equation over one half-cycle, starting in the ground state. The propagation in the electric field $E \cos \omega t$ with $\omega = 0.057$ au and $E = 0.14$ continues until $\omega t = 2\pi$. With such a set-up, the first recollision is completed, the later returns have not occurred yet, and the vector-potential $A(t) = -v_0 \sin \omega t$ is equal to zero at the turn-off, resulting in the zero velocity shift due to the instantaneous turn-off.

Figure 2(a) shows the $|\Psi|$ at $\omega t = 2\pi$ in the velocity space. Figure 2(b) shows the calculation for an identical initial condition for a single scattering centre $V = -1.3/\sqrt{x^2 + y^2 + a^2}$ which provides an atomic-like reference with the same ionization potential. As expected, the spectrum lies on the circle with a shifted origin. The circular cut (figure 2(c)) has the diffraction minima and maxima at the expected positions. The triple-peaked structure of the zero-order maximum is due to the holographic-type interference, which is also present in the reference atomic-like signal and disappears when the transverse velocity width is set to zero by setting $\Psi(x, y) = \Psi(x, 0)$ at $\omega t^* = \pi/2$. The hologram region is narrow due to narrow transverse distribution in the initial wave packet.

Having learned how to make proper cuts and how to identify holograms, we can now analyse laser-induced interference of different trajectories in the final spectrum.

Direct versus rescattered trajectories. The amplitude $a(\mathbf{v})$ to detect an electron with velocity \mathbf{v} has contributions from both direct (no recollision) and rescattered electrons: $a = a_d + a_r$. The energy spectrum of the direct electrons has a cut-off at $2U_p$ and is narrowly focused along

the laser polarization, see [8] and equation (2). The holographic interference is also present there. Outside this region, we only deal with rescattered trajectories and their interference.

Interference of long and short rescattered trajectories. In the strong field limit, the amplitude $a_r(\mathbf{v})$ factorizes into the product of the amplitudes of the consecutive processes of tunnel ionization a_{ion} , propagation in the laser field a_{pr} , scattering a_{sc} and propagation to the end of the pulse:

$$a_r(v_x, v_y) = \sum_t a_{\text{ion}}[t_0(t)] a_{\text{pr}}[t_0(t) \rightarrow t] \times a_{\text{sc}}[(v(t), 0) \rightarrow (v_x - v_0 \sin \omega t, v_y)] a_{\text{pr}}[t \rightarrow \infty]. \quad (7)$$

The summation is carried over all moments of recollision t which lead to the same final v_x, v_y . In contrast to standard above-threshold ionization, where such an interference of ‘quantum trajectories’ (see, e.g., [10]) is studied for a given *final* energy, here the angular pattern is taken at a given *recollision* energy. Such $t = \text{const}$ cuts do not correspond to a fixed final energy, changing the set of interfering trajectories: one of the moments t in the sum equation (7) is fixed for all v_x, v_y , others change as we change v_x, v_y along the cut.

To minimize the number of interfering trajectories, in our simulations we use phase-stabilized nearly single-cycle pulses with zero carrier-envelope phase, $E(t) = Ef(t) \cos \omega t$. This suppresses contributions of rescattered trajectories that start with phases other than $0 < \omega t_0 < \pi/2$, as well as the contributions of late and multiple returns. However, this does not eliminate the interference of two trajectories that start within the same quarter-cycle ($0 < \omega t_0 < \pi/2$) and return within the same cycle ($\omega t < 2\pi$). These are the short ($\omega t < \phi^*$) and long ($\omega t > \phi^*$) trajectories, where $\phi^* \simeq 4.4$ is the phase of the highest energy trajectory ($3.17U_p$). The key problem for diffraction related to these trajectories is that their recollision energies are different.

We can identify the interfering trajectories and phases for given v_x, v_y using equation (6). For brevity, we drop the small term $\gamma^2 dt_0/dt$, which makes our analysis I_p independent. In the dimensionless variables $\mathbf{u} = \mathbf{v}/v_0$, immediately after scattering the outgoing velocity in the x direction is $u_x^{(\text{out})} = \pm \sqrt{(\sin \omega t_0 - \sin \omega t)^2 - u_y^2}$ for the forward (+) and backward (−) elastic scattering. Here ‘forward’ and ‘backward’ mean that, without the laser field, the scattering angle would have been below or above $\pi/2$. Velocity at the detector is

$$u_x = u_x^{(\text{out})} + \sin \omega t = \sin \omega t \pm \sqrt{(\sin \omega t_0(t) - \sin \omega t)^2 - u_y^2} \equiv F^\pm(\omega t, u_y). \quad (8)$$

The functions $F^\pm(\phi, u_y)$ versus ϕ are shown in figure 3(a) for $u_y = 0.9$. For each v_y , $F^\pm(\phi, u_y)$ form a loop which means that there are always two different moments of return, corresponding to the same final v_x . Note that the corresponding energies of return (figure 3(a)) are different. The horizontal lines separate different regions of interference: forward–forward (FF) between two forward scattered trajectories, backward–backward (BB) between two backward scattered trajectories and forward–backward (FB) between one of each. Local maxima (minima) of F^+ (F^-) define the energy cut-offs for each value of v_x . Figure 3(b) combines such points to show the classical cut-off of the angle-resolved spectrum and different areas of interference. A dashed circle in figure 3(b) is the cut for $\phi \simeq 4.4$ (recollision energy $\simeq 3.17U_p$), which contains no interference in the ‘BB’ area.

Figures 4 show numerical simulations of the time-dependent Schrödinger equation for the model potential equation (1), with the peak field $E = 0.14$ au and $\omega = 0.057$ au. Panel (a) shows the electron spectrum for 1.25 cycle long $\cos \omega t$ pulse with constant amplitude. The pulse starts at $\omega t = -\pi/2$ and ends at $\omega t = 2\pi$. The ground state is projected out at $\omega t = \pi/2$.

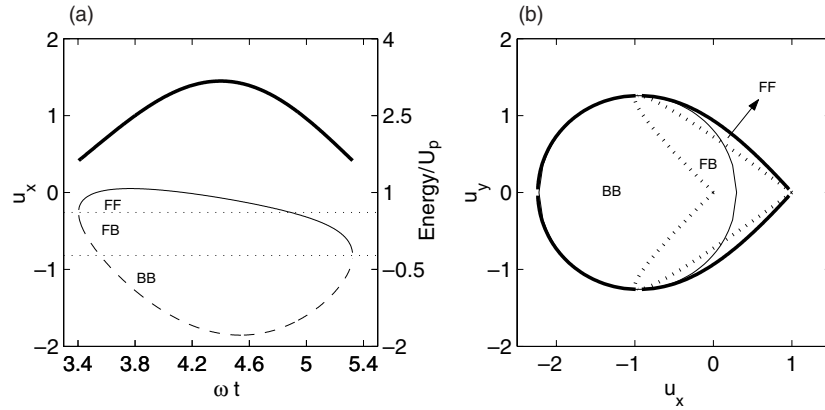


Figure 3. (a) Velocities u_x of forward F^+ (solid line) and backward F^- (dashed line) scattering as a function of the return phase $\phi = \omega t$, for $u_y = 0.9$. The thick solid line shows the return energy. Dotted lines separate three regions of interference marked as FF, FB and BB (see text). (b) Classical cut-off of the angle-resolved spectrum (solid line) and a circular cut for the recollision phase $\phi = 4.4$ (recollision energy $\simeq 3.17U_p$).

Therefore, (i) the ionization occurs predominantly during the half-cycle $-\pi/2 < \phi_0 < \pi/2$, (ii) interference of long and short trajectories is not obscured by multiple returns and (iii) terminating the pulse abruptly at $\omega t = 2\pi$ causes no shift in the free electron velocity. The shape of the angle-resolved spectrum is the same as expected from the analytical analysis shown in figure 3(b). The interference of long and short trajectories leads to high-frequency (the corresponding phase difference scales as U_p/ω) ring-like structures in figures 4(a) and (c). It does not mask the diffraction pattern, which is clearly visible along the cut corresponding to the maximum recollision energy in figure 4(a) (see figure 4(b)).

Panels (c) and (d) show simulations for a short pulse with the envelope $f(t) = \cos^2(\pi t/2T)$ for $-T < t < T$ and $f(t) = 0$ otherwise, for $T = 5$ fs (FWHM = 5 fs). The diffraction pattern is still clear along similar cuts, see panel (d). Note that we have two overlapped spectra similar to figure 4(a), one reflected through $v_y = 0$. They originate from ionization events near $\omega t_0 = 0$ (left-hand image) and near $\omega t_0 = -\pi/2$ (right-hand image). The images are not mirror-symmetric, as would have been the case for the long pulse. The first ionization event near $\omega t_0 = -\pi/2$ has lower probability but higher recollision energy due to the minimal change of the envelope during the oscillation. For the second ionization event, the maximum recollision energy is reduced by the quickly decreasing envelope.

The ring-like structures in the interference of long and short trajectories can be reproduced by the stationary phase analysis equation (7) (which contains no contribution from direct electrons and hence no hologram). Figure 5 shows

$$\aleph(\mathbf{v}) = \left| \sum_n \exp \left[-iS_1(t^{(n)}, t_0^{(n)}) - iS_2(\mathbf{v}, T, t^{(n)}) + iI_p t_0^{(n)} \right] \right|^2, \quad (9)$$

which singles out the interference by setting weights associated with ionization and scattering to unity and omitting the structural (diffraction) contribution. The summation index $n = 1, 2$ goes over the two trajectories that start at $0 < \omega t_0 < \pi/2$ and end up with the same final velocity \mathbf{v} . The corresponding moments of recollision $t^{(n)}$ are found from equation (6) (neglecting the γ^2 term), and $t_0^{(n)} = t_0(t^{(n)})$ are the solutions of equation (4). The actions accumulated before

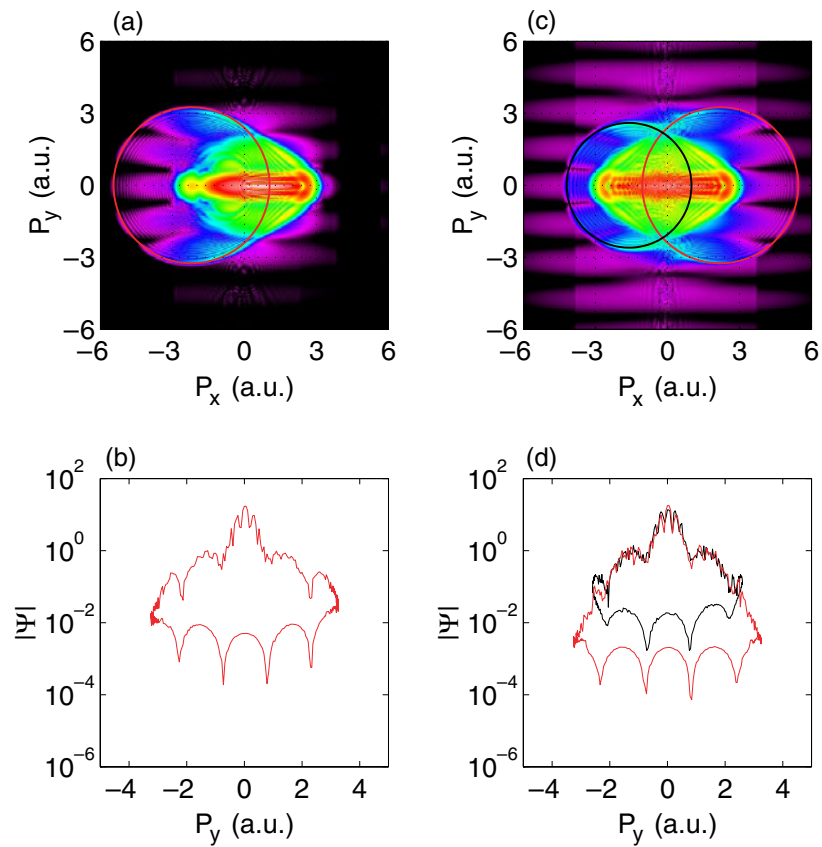


Figure 4. (a) Electron spectrum $|\Psi(v_x, v_y)|$ for a 1.25 cycle pulse with a constant amplitude, $E = 0.14$ au ($I \approx 6.9 \times 10^{14}$ W cm $^{-2}$ and $\lambda = 800$ nm, each new colour represents the order of magnitude); (b) spectral cut for a fixed moment of recollision ($\omega t \approx 4.4$); (c), (d) same as (a), (b) but for a 5 fs pulse $f(t) = \cos^2(\pi t/2T)$, $T = 5$ fs.

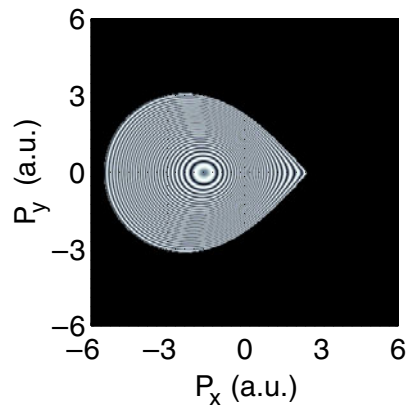


Figure 5. Analytical results emphasizing ring-like structures in figure 4(a) caused by the interference of short and long trajectories.

and after the recollision are

$$\begin{aligned} S_1(t, t_0) &= \frac{1}{2} \int_{t_0}^t dt' [-v_0 \sin \omega t' + v_0 \sin \omega t_0]^2 \\ S_2(\mathbf{v}, T, t) &= \frac{1}{2} \int_t^T dt' [\mathbf{v} - \mathbf{e}_x v_0 \sin \omega t_0]^2. \end{aligned} \quad (10)$$

The number of interference fringes counted along the $v_y = 0$ cut in figure 5 is only slightly less than that counted in figure 4(a). We currently attribute this small difference to the effects of the Coulomb potential.

Thus, despite a series of complications, the diffraction image of the parent molecule can be distilled out of the electron spectrum generated by intense-field ionization.

One of the most interesting directions suggested by this work is the opportunity to use holographic structures to image the molecule. Unlike diffraction, the hologram records both the magnitude *and* phase of the scattering amplitude. In the present calculation, the hologram barely distinguishes atom from molecule: the molecule is aligned perpendicular to the laser field, and the initial spread in the transverse velocity is too small to provide sufficient spatial resolution. However, changing the alignment of the molecule would allow one to use the large longitudinal velocity component for holography, increasing the resolution. Another possibility is to use elliptical polarization, either constant or time dependent, to move the wave packet by its half-width along the molecular axis, enhancing the holographic signal near the first maximum while retaining the zero maximum. One can also stretch the molecule.

Acknowledgments

We acknowledge stimulating discussions with S Patchkovskii, S Yurchenko, G Yudin, M Lein, P Knight, J Marangos and Yu Denisjuk. OS acknowledges financial support from the Lise Meitner Foundation. OS and MS acknowledge stylographic support from ONYX Uni-Ball. MS and MI acknowledge financial support from NSERC and the NRC Graduate Student Supplement programme; MI and OS acknowledge financial support by the NSERC International Opportunity Fund.

References

- [1] Zuo T, Bandrauk A D and Corkum P B 1996 *Chem. Phys. Lett.* **259** 313
- [2] Lein M, Marangos J and Knight P 2002 *Phys. Rev. A* **66** 051404
- [3] Niikura H, Legare F, Hasbani R, Bandrauk A D, Ivanov M Yu, Villeneuve D M and Corkum P B 2002 *Nature* **417** 917
- [4] Ihee H, Lobastov V, Gomez U, Goodson B, Srinivasan R, Ruan C-Y and Zewail A 2001 *Science* **291** 458
- [5] Corkum P B 1993 *Phys. Rev. Lett.* **71** 1995
- [6] Stapelfeldt H and Seideman T 2003 *Rev. Mod. Phys.* **75** 543
- [7] Yurchenko S N, Patchkovskii S, Litvinyuk I V, Corkum P B and Yudin G L *Phys. Rev. Lett.* submitted
- [8] Delone N and Krainov V 1994 *Multiphoton Processes in Atoms* (Berlin: Springer)
- [9] See, e.g., Yakovlev V and Scrinzi A 2003 *Phys. Rev. Lett.* **91** 153901
- [10] See, e.g., Kopold R, Milosevic D B and Becker W 2000 *Phys. Rev. Lett.* **84** 3831